Available online at www.sciencedirect.com
ScienceDirect
Thin Solid Films 516 (2008) 3665–3668
www.elsevier.com/locate/tsf

Synthesis and characterization of crystalline β-Bi_2O_3 nanobelts

Hyoun Woo Kim *

School of Materials Science and Engineering, Inha University, Incheon 402-751, Republic of Korea

Available online 17 August 2007

Abstract

We synthesized β-Bi_2O_3 nanobelts on silicon substrates without using a metal catalyst. Trimethylbismuth and O_2 were taken as the source of bismuth and oxygen, respectively. X-ray diffraction and transmission electron microscopy studies confirmed the formation of tetragonal Bi_2O_3 phase. The typical width of the β-Bi_2O_3 nanobelts was in the range of 40–400 nm. We suggested that the growth of β-Bi_2O_3 nanobelts was mainly controlled by a vapor–solid mechanism. Photoluminescence measurements at room temperature exhibited a visible light emission band peaking at around 2.81 eV.

Keywords: Nanobelts; β-Bi_2O_3; Vapor–solid process; MOCVD

1. Introduction

The fabrication of Bi-containing materials has been studied intensively owing to their remarkably useful solid-state properties and their applications in several technological fields [1,2]. Particularly, bismuth oxide (Bi_2O_3) has been of great interest due to the significant energy band gap (2.85 and 2.58 eV for the monoclinic α-Bi_2O_3 and tetragonal β-Bi_2O_3 phases, respectively), high refractive index, high dielectric permittivity, and marked photoconductivity [3–5]. Therefore, it can be used not only for gas sensor technology [6,7], but also for optical coatings, microelectronics, and ceramic glass manufacturing [8–10].

Nanometer-scale one-dimensional (1D) materials, such as nanowires, nanotubes, and nanobelts, have attracted much attention due to their unique properties and promising applications in the electrical, optical, and magnetic devices and among them, the belt-like nanomaterial may be an ideal system for fully understanding dimensionally confined transport phenomena and fabricating functional nanodevices, due to its special morphology and a significant modification of the transport and optical properties. The finite size of the belt could confine the electrons wave functions, resulting in quantized energy levels. In addition, the greatly enhanced surface-to-volume ratio augments the role of surface states in the sensor applications.

Although nanobelts of various metal oxides, such as ZnO [11], SnO_2 [12], Ga_2O_3 [13], In_2O_3 [14], and MgO [15] have been successfully synthesized, to the best of our knowledge, production of Bi_2O_3 nanobelts has not been reported to date. In this research, we report a chemical vapor deposition (CVD) route to β-Bi_2O_3 nanobelts. Among the various polymorphs of Bi_2O_3 (such as α-, β-, γ-, δ-, and ω-Bi_2O_3), β-Bi_2O_3 is a metastable phase, which exhibits a promising ionic conductivity by the deliberate doping [16,17]. We speculated on the growth mechanism of Bi_2O_3 nanobelts. In addition, we investigated the structural and photoluminescence (PL) properties of the product. The growth of nanomaterials onto the silicon (Si) substrate without using metal catalyst may contribute to integration of future devices with developed Si integrated circuit technology.

2. Experimental

Bi_2O_3 nanobelts have been grown in a cold wall reactor by the metalorganic chemical vapor deposition (MOCVD) system described previously [18]. As a starting material, we used standard polished p-type (1 0 0) Si wafers. The Si substrate was cut into small pieces with dimensions of 20 mm × 20 mm, which was precleaned with organic solvents and subsequently blow-dried in N_2 gas. In the growth process, we used trimethylbismuth (TMBi) ($Bi(CH_3)_3$, boiling point = 108.8 °C [19]) and O_2

* Tel.: +82 32 860 7544; fax: +82 32 862 5546.
E-mail address: hwkim@inha.ac.kr.

0040-6090/$ - see front matter © 2007 Elsevier B.V. All rights reserved.
doi:10.1016/j.tsf.2007.08.042

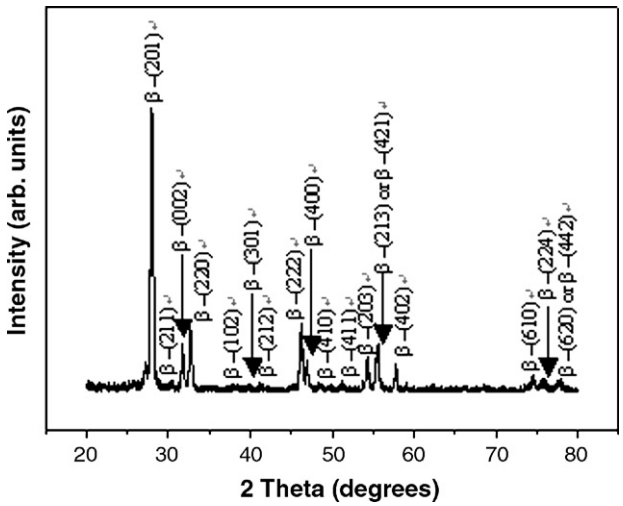

Fig. 1. Typical XRD pattern of the product. The numbers above the peaks correspond to the (*hkl*) values of the tetragonal Bi_2O_3 structure.

as the source of bismuth and oxygen, respectively. The flow rate of O_2 was 10 standard cubic centimeters per minute (sccm). In addition, we employed argon (Ar) as a carrier gas for TMBi, and kept its flux at 20 sccm during the growth process. The pressure of the chamber during the growth was about 1 Torr. The temperature of the substrate was 450 °C and the growth time was 1 h. The bubbler of TMBi was maintained at −2 °C.

The products were characterized by various techniques. X-ray powder diffraction (XRD) pattern was recorded by employing a Philips X'pert X-ray diffractometer with a CuKα radiation source (λ=0.154056 nm). Scanning electron microscopy (SEM) images were obtained using a field emission SEM (FE-SEM, Hitachi S-4200). The morphology of the as-prepared products was observed by transmission electron microscopy (TEM). The TEM was carried out on a Philips CM-200 instrument with an accelerating voltage of 200 kV. The high resolution TEM (HRTEM) image, the energy-dispersive X-ray spectroscopy (EDX) spectrum, and the selected area electron diffraction (SAED) pattern were also taken on the same microscope. TEM samples were prepared by dispersing as-prepared sample onto a carbon-coated copper grid. PL spectroscopy was used for their optical characterization at room temperature, using a continuous wave He–Cd laser of 3.82 eV in energy as the excitation source. The spectrum was measured with a SPEC-1403 photoluminescence spectrometer.

3. Results and discussion

The phase and the purity of the product were determined from the XRD pattern shown in Fig. 1. Miller indices of tetragonal Bi_2O_3 structure were marked in this pattern. All recognizable diffraction peaks in the pattern can be indexed to tetragonal β-Bi_2O_3 structure with lattice parameters of a=7.742 Å and c=5.631 Å, which are in good agreement with those of bulk tetragonal Bi_2O_3 crystal (JCPDS Card No. 27-0050). In the present XRD measurements, the angle of the incident beam to the substrate surface was about 0.5°, with detector being rotated to scan the samples. Therefore, we suppose that the reflection peaks are mainly from the product. It is noteworthy that no characteristics peaks of other crystalline impurities were detected within the detection limit, indicating that well-crystallized Bi_2O_3 can be obtained through the present synthesis route.

We have examined the morphology and size of the resulting product by observing the SEM images. Fig. 2a shows a plan-view SEM image of the deposits on the substrate surface, showing an agglomeration of 1D nanomaterials over a large area. Fig. 2b shows an SEM image of the side view of the deposits, revealing the random length directions of the 1D nanomaterials. Statistical analysis of many SEM images shows that the 1D nanomaterials have widths or diameters ranging from 40 to 400 nm and lengths up to several tens of micrometers. Fig. 2c shows an enlarged SEM image of the 1D nanomaterials. The arrowheads indicate the semi-transparent natures of the nanomaterials, suggesting that their geometrical shapes are belt-like. The nanobelt has an almost uniform width along the length direction and a smooth surface. Also, close examination revealed that the nanobelts had thicknesses less than 1/5 of the widths.

TEM was employed for further structural study of the sample. Fig. 3a shows the TEM image of a single nanobelt. The contrast observed in the TEM image is presumably due to strain resulting from twisting or bending of the belt-like structure. Fig. 3b shows the SAED pattern taken from an individual nanobelt. The SAED shows a spotty pattern, which means that as-

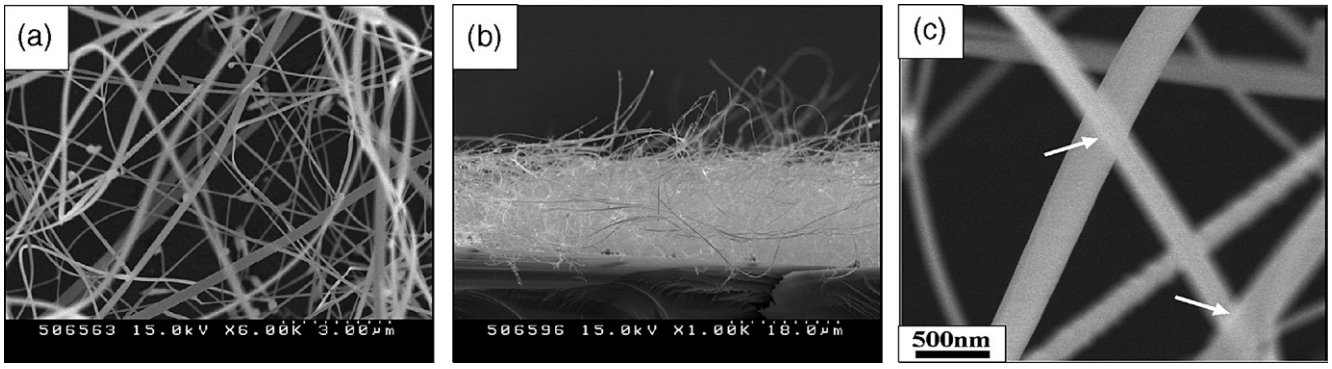

Fig. 2. (a) Plan-view and (b) Side-view SEM images of the product. (c) Enlarged SEM image, in which the semi-transparent nature of the nanobelt is marked with arrows.

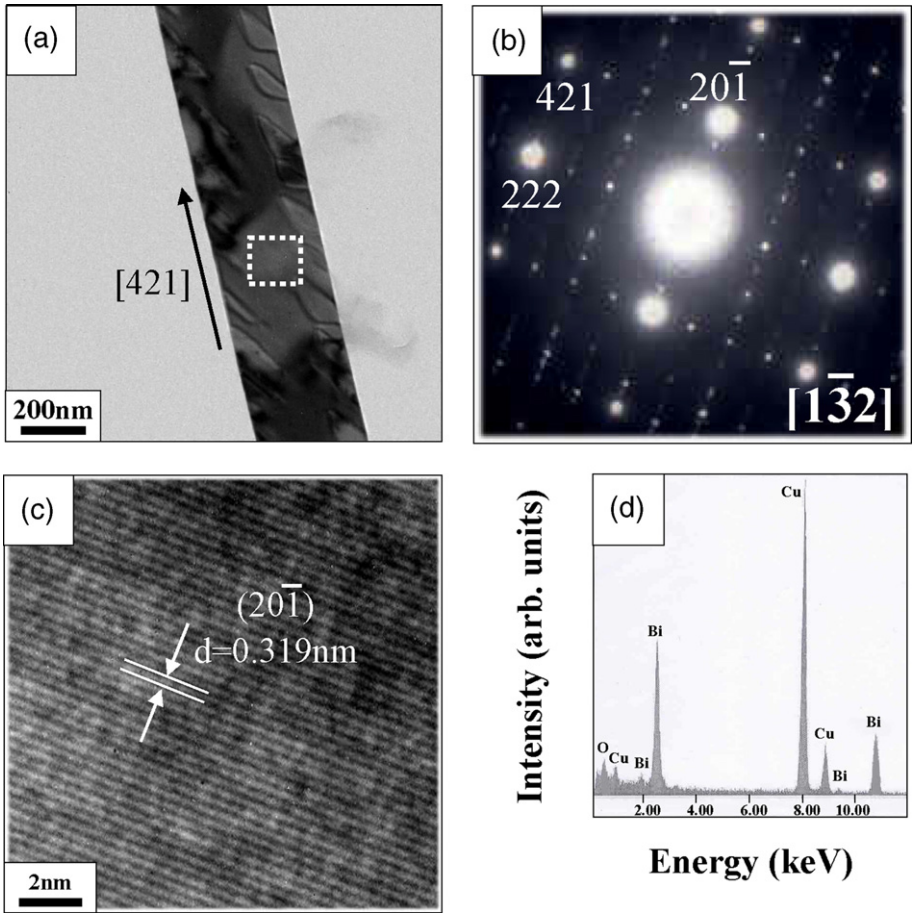

Fig. 3. (a) TEM image of a β-Bi_2O_3 nanobelt. (b) Typical diffraction pattern that was obtained by focusing the electron beam on an individual nanobelt. (c) HRTEM image enlarging the selected part in (a). (d) EDX spectrum of a β-Bi_2O_3 nanobelt. The Cu shown in the spectrum originates from the TEM Cu grid.

prepared nanobelts are well crystallized. The diffraction spots can be indexed to the (222), (421), and (20$\bar{1}$) planes with the [1$\bar{3}$2] zone axis, confirming the formation of tetragonal β-Bi_2O_3 phase. It also shows the presence of additional weaker superlattice reflections, presumably due to the long-range ordering of the oxygen sublattice. Similar superlattice reflections have been observed in δ-Bi_2O_3 lattices [20]. Fig. 3c shows an HRTEM image enlarging an area enclosed by the dotted square in Fig. 3a, revealing a good crystallinity. A lattice space with value of about 0.319 nm was calculated, which is corresponding to the (20$\bar{1}$) plane of tetragonal β-Bi_2O_3. The length direction of the nanobelt is its <421> lattice direction, as shown in Fig. 3a. From the corresponding EDX microanalysis, we observe that not only the stem part but also the tip part of the nanobelt contained only Bi and O elements. The corresponding EDX data for the tip part of nanobelt is given in Fig. 3d. The peak of element Cu (marked in Fig. 3d) is obtained from the copper grid on which these Bi_2O_3 nanobelts were supported.

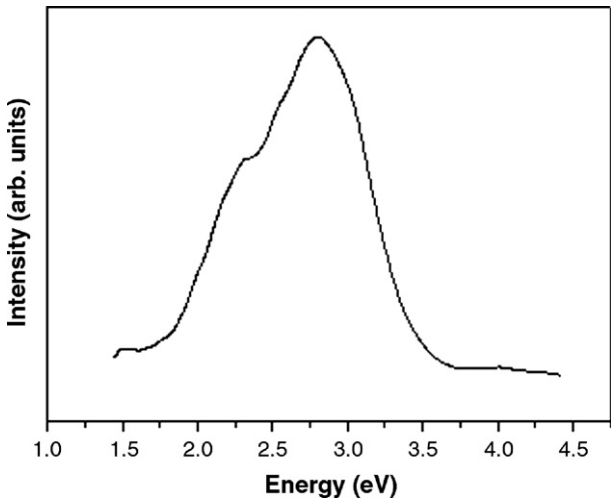

Fig. 4. Photoluminescence spectrum recorded at room temperature on the product. The light source was 325 nm-wavelength line from a He–Cd laser.

It is known that the vapor–solid (VS) and vapor–liquid–solid (VLS) are the two main mechanisms for the vapor-phase-involved formation of 1D nanomaterials [21–24]. No metal was employed as the catalyst in our synthetic process, and no metal element other than Bi and Cu was detected on the ends of the 1D nanomaterials from EDX analysis. Also, although it is not shown in this paper, SEM and TEM investigations showed that no catalyst heads were found the tips of the nanobelts. As a result, the catalyst-induced VLS mechanism may be ruled out. Therefore, it is likely that the growth of Bi_2O_3 nanobelts follows the mechanism similar to the VS mechanism. At the beginning of the MOCVD process at 450 °C, we suppose that the TMBi vapors were generated from the TMBi bubbler, with being

carried by inert Ar gas. The TMBi vapors or decomposed vapor reacts with O_2 gas, ultimately forming the solid Bi_2O_3 on the substrate. Although detailed investigation on the growth mechanism is now in progress, we surmise that the present synthetic process may be under the condition at which the anisotropic 1D growth was favored.

To the best of our knowledge, nothing is known about the PL of bismuth oxides belt-like structures. Fig. 4 shows the room-temperature PL emission spectrum from the as-synthesized product upon photoexcitation at 3.82 eV. There is a strong PL emission band located around 2.81 eV in the blue region with a shoulder at about 2.31 eV. A similar blue emission has been previously reported from Bi_2O_3 nanoparticles [25]. The observed blue light emission may be attributed to a recombination from the conduction band to the energy levels of deep-traps or surface states, originating from crystal defects inside or at the surface of the nanobelts. The origin of the shoulder at about 2.31 eV is not clear at this moment and needs more investigation.

4. Conclusion

In summary, we have demonstrated the preparation of β-Bi_2O_3 nanobelts without assistance of a metal catalyst using a reaction of a TMBi and O_2 mixture. SEM images indicate that the product consists of 1D nanomaterials, with a significant amount of belt-shaped structures. XRD, SAED and HRTEM investigations reveal that the nanobelts are crystalline with a tetragonal β-Bi_2O_3 structure. We propose that the growth mechanism of β-Bi_2O_3 nanobelts is dominated by a VS process. The blue light emission at 2.81 eV was detected for the as-synthesized product, which suggests the potential applications to optoelectronic nanodevices.

Acknowledgement

This work was supported by the Inha Research Fund 2006t.

References

[1] N. Hykaway, W.M. Sears, R.F. Frindt, S.R. Morrison, Sens. Actuators 15 (1988) 105.
[2] A.S. Poyossian, H.V. Abovian, P.B. Avakian, S.H. Mkrtchian, V.M. Haroutunian, Sens. Actuators, B, Chem. 4 (1991) 545.
[3] V. Dolocan, F. Iova, Phys. Status Solidi, A Appl. Res. 64 (1981) 755.
[4] L. Leonite, M. Caraman, G.I. Rusu, J. Optoelectron. Adv. Mater. 2 (2000) 385.
[5] L. Leonite, M. Caraman, M. Alexe, C. Harnagea, Surf. Sci. 507–510 (2002) 480.
[6] Z.N. Adamian, H.V. Abovian, V.M. Aroutiounian, Sens. Actuators, B, Chem. 35–36 (1996) 241.
[7] T. Hyodo, E. Kanazawa, Y. Takao, Y. Shimizu, M. Egashira, Electrochemistry 68 (2000) 24.
[8] M. Schuisky, A. Härsta, Chem. Vap. Depos. 2 (1996) 235.
[9] G. Bandoli, D. Barecca, E. Brescacin, G.A. Rizzi, E. Tondello, Chem. Vap. Depos. 2 (1996) 238.
[10] A. Pan, A. Ghosh, J. Non-Cryst. Solids 271 (2000) 157.
[11] Y.B. Li, Y. Bando, T. Sato, K. Kurashima, Appl. Phys. Lett. 81 (2002) 144.
[12] J.Q. Hu, X.L. Ma, N.G. Shang, Z.Y. Xie, N.B. Wong, C.S. Lee, S.T. Lee, J. Phys. Chem., B 106 (2002) 3823.
[13] G. Gundiah, A. Govindaraj, C.N.R. Rao, Chem. Phys. Lett. 351 (2002) 189.
[14] C. Liang, G. Meng, Y. Lei, F. Phillipp, L. Zhang, Adv. Mater. 13 (2001) 1330.
[15] Y. Li, Y. Bando, T. Sato, Chem. Phys. Lett. 359 (2002) 141.
[16] Z. Wuzong, D.A. Jefferson, M. Alario-Franco, J.M. Thomas, J. Phys. Chem. 91 (1987) 512.
[17] V.V. Kharton, E.N. Naumovich, A.A. Yaremchenko, F.M.B. Marques, J. Solid State Electrochem. 5 (2001) 160.
[18] H.W. Kim, N.H. Kim, Appl. Phys., A Mater. Sci. Process. 81 (2005) 763.
[19] K. Michalke, J. Meyer, A.V. Hirner, R. Hensel, Appl. Organomet. Chem. 16 (2002) 221.
[20] E.D. Wachsman, S. Boyapati, M.J. Kaufman, J. Am. Ceram. Soc. 83 (2000) 1964.
[21] R.S. Wagner, W.C. Ellis, Appl. Phys. Lett. 4 (1964) 89.
[22] Z.W. Pan, Z.R. Dai, Z.L. Wang, Science 291 (2001) 1947.
[23] G.W. Sears, Acta Metall. 3 (1956) 268.
[24] A.P. Levitt, Whisker Technology, Wiley, New York, 1970.
[25] W. Dong, C. Zhu, J. Phys. Chem. Solids 64 (2003) 265.